Photonic Network Communications (2022) 43:147–155
https://doi.org/10.1007/s11107-021-00959-3

ORIGINAL PAPER

MUX/DEMUX circuit using plasmonic antennas for LiFi and WiFi uplink and downlink transmission

A. Garhwal[1] · A. E. Arumona[2] · K. Ray[3] · P. Youplao[4] · S. Punthawanunt[5] · P. Yupapin[6]

Received: 26 November 2020 / Accepted: 14 November 2021 / Published online: 16 January 2022

Abstract

A microring-embedded Mach–Zehnder interferometer (MZI) system is proposed to form the multiplexing (demultiplexing) for wireless and light fidelity (WiFi and LiFi) uplink and downlink transmission. The system consists of two center microrings at the transmitter and a center microring at the receiver with two small rings along the sides of the center microrings. The whispering-gallery mode (WGM) is formed by the nonlinearity effect induced by the two small rings with suitable parameters. The embedded gold gratings are excited by the WGM, where the plasmon oscillation and electron density are obtained. All possible multiplexing/demultiplexing (MUX/DEMUX) schemes based on space–time input can be applied. The transmission is performed using the tested node. The uplink and downlink input source wavelengths of 1.10 μm and 1.30 μm for LiFi and WiFi are manipulated. The manipulated tested node is employed with a maximum length of 1, 000 km away from the transmitted point via a fiber optic cable. The results obtained have shown that the optimum transmission bit rate of 2.52 Petabit s^{-1} with the optimum bit error rate (BER) of 0.38 is obtained.

Keywords Photonic circuits · Plasmonic circuit · MUX-DEMUX · Spin-wave transmission · MZI · Plasmonic Antenna

1 Introduction

The Mach–Zehnder interferometer (MZI) is an optical device where one input signal propagates equally through the two arms. The output signals are combined and transmitted, where there is a π/2 phase difference between the signals. MZI multiplexing is allowed to have additional components, which is suitable for modern technology. Moreover, the electro-optical components can be added due to reliability, small size, and utilized for all multiplexing and demultiplexing applications. MZI has many applications like in photonic crystals [1], wavelength conversion on cross-polarization modulation [2], optical switch [3, 4], optical buffer and OR gate [5], humidity sensor [6], electro-optic switch/filter [7], graphene-based splitter/switch [8], DE multiplexer [9], and antennas [10]. Various applications are also reported. The use of all-optical multiplexing and demultiplexing for C-band wireless transmission was proposed, where the system was suitable for an integrated optical circuit to interconnect [11], where the polarization multiplexing is applied to enhance the capacity of the optical link for 5G [12]. Tapered multicore fiber coupling efficiency using mode division multiplexing (demultiplexing) is reported [13] based on total reflection switches, all-optical frequency

✉ K. Ray
kray@jpr.amity.edu

✉ P. Yupapin
preecha@techsakon.ac.th

P. Youplao
phichai.yo@rmuti.ac.th

1 Amity School of Engineering and Technology, Amity University Rajasthan, Jaipur, India

2 Division of Computational Physics, Institute for Computational Science, Ton Duc Thang University, Ho Chi Minh City, Vietnam

3 Amity School of Applied Sciences, Amity University Rajasthan, Jaipur, India

4 Department of Electrical Engineering, Faculty of Industry and Technology, Rajamangala University of Technology Isan Sakon Nakhon Campus, Sakon Nakhon, Thailand

5 Faculty of Science and Technology, Kasem Bundit University, Bangkok, Thailand

6 Department of Electrical Technology, School of Industrial Technology, Institute of Vocational Education Northeastern Region 2, Sakonnakhon, Thailand

encoded multiplexer and demultiplexing to increase the ultra-high processing speed [14]. Similarly, wavelength division multiplexing [15] and polarization division multiplexing were also presented [16]. Optical filter analysis for demultiplexing of all-optical OFDM systems was presented, where the different optical filters using Gaussian, rectangular, Bessel and sinc forms are used [17]. The high-speed transmission of 160 Gb speed was achieved using optical time-division multiplexing based on MZI switching [18]. The electro-optic system was applied as a plasmonic switch for the high-speed optical amplifier and optical computing using energy-efficient switching and a ripple carrier adder, respectively [19–21]. The micro-MUX/DEMUX devices can be applied and linked by the optical cable in the communications [22, 23]. More works reported the use of MZI in other forms [24, 25], in which the use of MZI embedded microring resonator has given promising applications. Generally, there are various works on LiFi and WiFi found in the references [26–30]. However, in this proposed work, the new scheme of the MUX/DEMUX using MZI has been presented. The system consists of two microring nodes embedded in the MZI coupled with two-phase modulators. The two center microrings act as the uplink and downlink transmitters. The space–time modulation is input; then, all MUX/DEMUX can be applied based on space–time modulation control. The transmission signals after MUX/DEMUX can perform the uplink and downlink via WGMs [31]. The simulation results are obtained by the two simulation programs, where firstly the system is designed in OptiFDTD software and simulated with the formation of whispering-gallery mode (WGM). Secondly, the data from the OptiFDTD is extracted, and the graphs are plotted in MATLAB. The simulated results are tested and interpreted for MUX/DEMUX transmission via a single-mode optical fiber connection.

2 Theoretical background

In Fig. 1, the input source is a dark soliton. The MZI divides the input light into two parts, which is the 50:50 coupler. The incoming light from the MZI is coupled with two panda ring resonators. In the proposed scheme, the polarized electrons are trapped and oscillated within plasmonic microring, which is in the form of WGM. The Bragg wavelength is formed, and the plasma frequency can be obtained.

A dark soliton is input in the propagation axis, which is explained by the following equation, which is given by [32, 33]

$$E_{\text{dark soliton}} = C \tanh\left[\frac{T}{T_0}\right] \exp\left[\frac{z}{2L_D} - i\omega_0 \mathrm{t}\right] \tag{1}$$

Here the soliton initial phase(t = 0) is neglected, and the Eq. (1) can be rewritten as:

$$E_{\text{dark soliton}} = C \tanh\left[\frac{T}{T_0}\right] \exp\left[\frac{z}{2L_D}\right] \tag{2}$$

where C is the optical field amplitude, and z is the propagation axis (distance). T is a soliton pulse propagation time in a frame moving with group velocity $T = \mathrm{t} - \beta_1 \mathrm{z}$, where β_1 and β_2 are the coefficients of linear and second-order terms of the Taylor expansion of propagation constant. The dispersion length of the soliton pulse is denoted by L_{D} and given as $L_D = T_0^2/\beta_2$, which is neglected. T_0 is the soliton pulse propagation time at the initial input.

The relationship between soliton and plasma of electron oscillation is given using the Drude model [34, 35], which is given by

$$\varepsilon(\omega) = 1 - \frac{n_e e^2}{\varepsilon_0 m \omega^2} \tag{3}$$

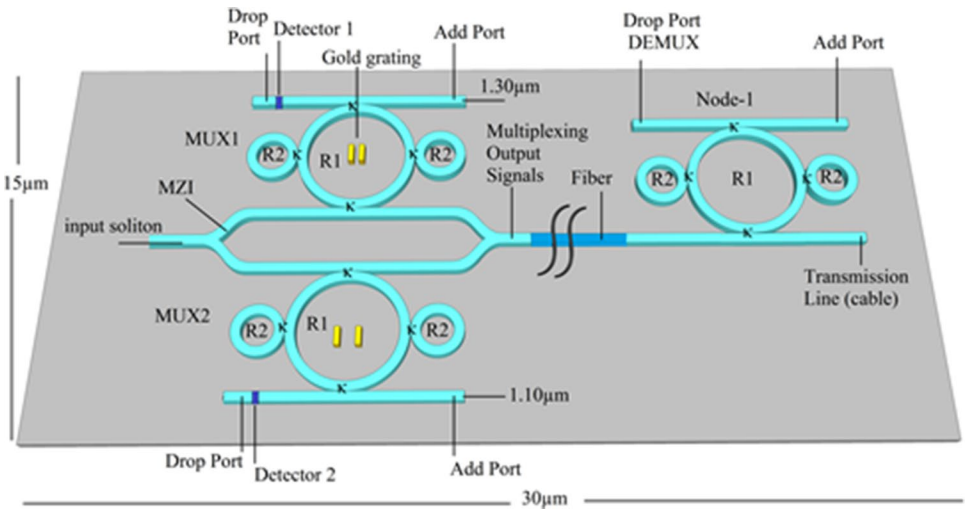

Fig. 1 The LiFi and WiFi uplink and downlink transmission, where MUX: multiplexing, DEMUX: demultiplexing, R1: center microring radius, R2: small ring (phase modulators) radii, κ: coupling constant. A soliton is input into the propagation axis (z)

where n_e, e, ε_0 and m are the electron density, electron charge, permittivity of free space and mass of electron, respectively. ω is the angular frequency. The plasma frequency is given by

$$\omega_p = \sqrt{\frac{n_e e^2}{\varepsilon_0 m}} \tag{4}$$

The first multiplexed equation is given by [36]

$$E_{addMUX1} = Fe^{\pm i2\pi \frac{c}{\lambda_1} t_1} \tag{5}$$

where c, λ_1 and t_1 are the speed of light in silicon, the space–time input wavelength (1.30 µm), and time. F is the amplitude. The ± sign indicates both sides of time. The MUX2 (lower microring) is similar to MUX1 (upper microring).

The second multiplexed equation is given by

$$E_{\text{addMUX2}} = \text{Fe}^{\pm i2\pi \frac{c}{\lambda_2} t_2} \tag{6}$$

where c, λ_2 and t_2 are the speed of light in silicon, the space–time input wavelength (1.10 µm), and time. The normalized output intensities of MUX1 and MUX2 are given by Eqs. (7) and (8).

$$\frac{I_{\text{drop MUX1}}}{I_{in}} = \left[\frac{E_{\text{dropMUX1}}}{E_{\text{dark soliton}}}\right]^2 \tag{7}$$

$$\frac{I_{\text{drop MUX2}}}{I_{in}} = \left[\frac{E_{\text{dropMUX2}}}{E_{\text{dark soliton}}}\right]^2 \tag{8}$$

The signal is transmitted using the optical fiber cable connection, which can be multiplexed/demultiplexed at the receiver. The obtained WGM can be controlled by the two small side rings, which act as phase modulators.

3 Results and discussion

This concept of the proposed system is that the electrons in the gold surface are trapped by the plasmonic waves, which is in the form of the whispering-gallery modes. The transmission of the trapped electrons is performed by the polarized waves (spin electron waves) via WiFi or LiFi. The system is designed, as shown in Fig. 1, which is simulated using the OptiFDTD software. By using suitable parameters, the whispering-gallery modes can be generated, which can be applied to form the plasmonic waves for electron excitation. Table 1 parameters are the optimized parameters, where the references are cited. The simulation uses a soliton with a wavelength of 1.54 µm, as shown in Fig. 1. The input signal is a dark soliton as given in Eqs. (1) and (2), and the

Table 1 Optimized parameters for simulation [34–37]

Parameters	Symbols	Values	Units
Dark soliton wavelength	λ_{d1}	1.54	µm
Modulated wavelengths	λ_1, λ_2	1.10,1.30	µm
Input power	P	10–30	mW
Center ring radius	R1	1.80	µm
Small rings radii	R2	0.80	µm
Coupling coefficient	κ	0.50	
Silica refractive index	n_{silica}	1.45	
Sio_2 refractive index	n_{sio_2}	3.42	
Si O_2 nonlinear refractive index	n_{osio_2}	2.7 x 10^{-16}	Cm^2 W^{-1}
Gold refractive index	n_{gold}	1.80	
Grating period	^1, ^2,^3	0.50, 0.40, 0.30	µm
Structure dimensions	L × W	30 × 15	μm^2
Waveguide loss	α	0.50	dB mm^{-1}
Effective core area	A_{eff}	0.30	μm^2
Single mode fiber lengths	L_{fiber}	10–1000	km
MZI-fiber coupling loss	–	0.1	dB
Fiber-node coupling loss	–	0.1	dB
Fiber loss	α_{fiber}	0.1	dB km^{-1}
Electron mass	m	9.11×10^{-31}	kg
Electron charge	e	1.6×10^{-19}	Coulomb
Free space permittivity	ε_0	8.85×10^{-12}	Fm^{-1}

3 dB coupler of the MZI arms divides the input signal into two equal parts. Micro-ring resonator (MRR) circuits are used in the upper and lower arms of the MZI. The MRR circuit consists of two center microrings of radius R1 and two small rings at the sides of each of the center microring of radius R2. The R1 microrings consist of the gold gratings embedded at the center microrings. The grating periods of the upper and lower microring-embedded gold gratings are different, which can generate different Bragg wavelengths that can be applied for uplink and downlink identifications. The add and drop ports are employed for multiplexing and demultiplexing signals of the upper and lower microrings, respectively. At the add port of the upper (MUX1) and lower (MUX2) MRRs, the multiplexing signals are given in Eqs. (5) and (6), where the wavelengths are 1.30 µm and 1.10 µm, respectively. The simulation is run for 20,000 steps to achieve the resonant results, where the output is normalized, as given in Eqs. (7) and (8). The required data are extracted from OptiFDTD simulation results and plotted in MATLAB. When light travels through the linear waveguide, it couples to the center ring. The light goes around the center ring, the nonlinearity effect (Kerr effect) is induced, and light is trapped inside the microring. The Kerr effect changes the refractive index of the silicon material, and the two side rings acting as phase modulators induce the nonlinearity (self-phase modulation), which varies the refractive index

of the silicon material. At resonance, the trapped light inside the center ring forms the WGM, as shown in Fig. 2a, where the WGMs are for uplink MUX1 (upper microring) and downlink MUX2 (lower microring). The excitation of the gold grating at the center ring, the free electrons in the gold grating oscillate with the incident light to form surface plasmons which propagate through the system with the intense electromagnetic field as shown in Fig. 2b. Electron density is obtained by using the Drude model, where the electron in the gold surface is excited by plasmonic waves and oscillated with the related plasma frequency as given by Eqs. (3) and (4). The wavelengths shift to two Bragg wavelengths of 1.56 µm and 1.57 µm, which can be used to form the plasma frequencies for antenna applications. The lower and upper microrings form the downlink and uplink antennas, which are employed for LiFi and WiFi connections. The LiFi employs the wavelength band, while the WiFi employs the frequency band. The transmission system can be formed and tested by the selected distance away linked by a fiber optic cable. Figures 3, 4 and 5show the plot of the WGM and drop port outputs of MUX1 and MUX2, in wavelength, frequency, and time domains. The multiplexed signals become input in a single-mode fiber cable, which acts as a medium between MUX (transmitter node) and DEMUX (receiver node). The fiber cable parameters and lengths are given in Table 1. Node-1 is a test node, where the multiplexed signals are demultiplexed and detected. Figure 6 shows the plot of the DEMUX outputs. Figure 7 shows the antenna profiles, where the uplink and downlink antenna gains are plotted with the input power, as shown in Fig. 7a. The input power is varied from 20 to 30mW. The uplink and downlink gains are 3.57 dB and 1.76 dB, respectively. Figure 7b–c shows the directivities of uplink and the downlink antennas. The uplink and downlink directivities are 12.53 and 12.41, respectively. The uplink and downlink frequencies are 195.2 THz and 195.9THz. In this work, the antenna directivity is dimensionless because no radiation intensity direction is specified [33]. Figure 7d–e shows the uplink and downlink frequency and wavelength bands for WiFi and LiFi, respectively. The quantum communication is also available by the spin-wave

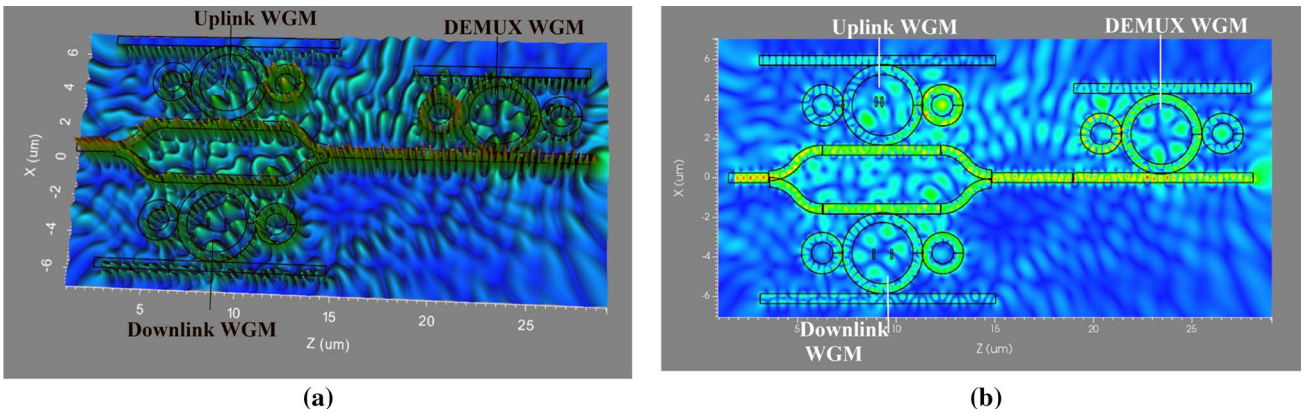

Fig. 2 The graphical result of WGMs using the Optiwave is observed at the uplink, downlink, and DEMUX WGM at 1.54 µm, where **a** formation of WGMs in the system, **b** electric field distribution within the system. The used parameters are given in Table-1, which are also applied in MATLAB. The center wavelengths shift to Bragg wavelengths 1.56 µm and 1.57 µm. Figure 2 **a** is the transmission of light through the device in terms of light intensity along z-axis, while Fig. 2 **b** is the electric field distribution of the trapped electrons along z axis. The number of mesh cells X is 259 and Mesh cells Z are 568 used in simulation

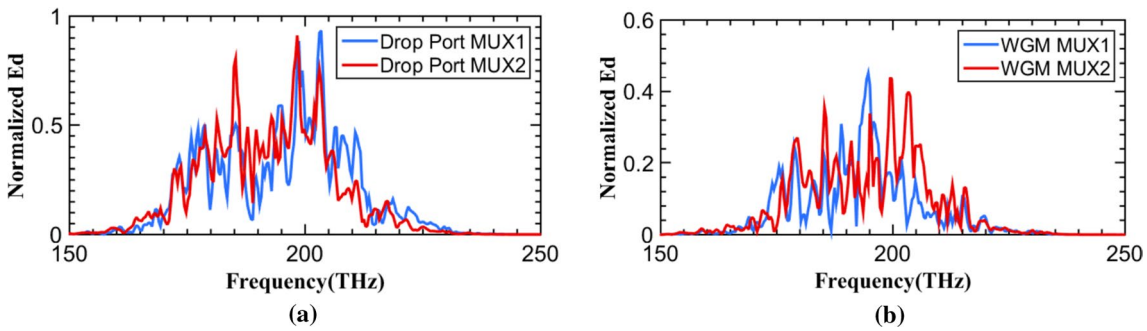

Fig. 3 Plot of the normalized electron density in frequency domain, where **a** drop port of MUX1 and MUX2, **b** WGM of MUX1and MUX2. The plasma frequencies are **a** 0.26×10^{16} radsec^{-1} and and **b** 1.83×10^{16} radsec^{-1} using an Eq. (4)

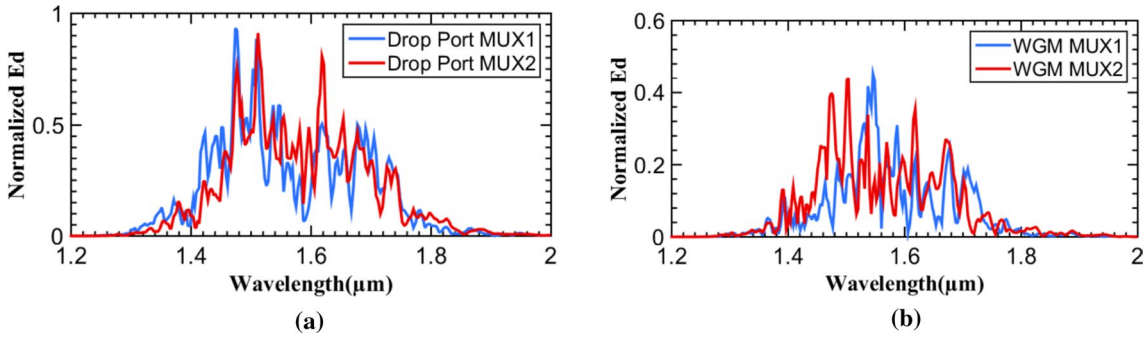

Fig. 4 Plot of the normalized electron density in wavelength domain, where **a** drop port of MUX1 and MUX2, **b** WGM of MUX1 and MUX2. The Bragg wavelengths are **a** 1.56 μm and **b** 1.57 μm

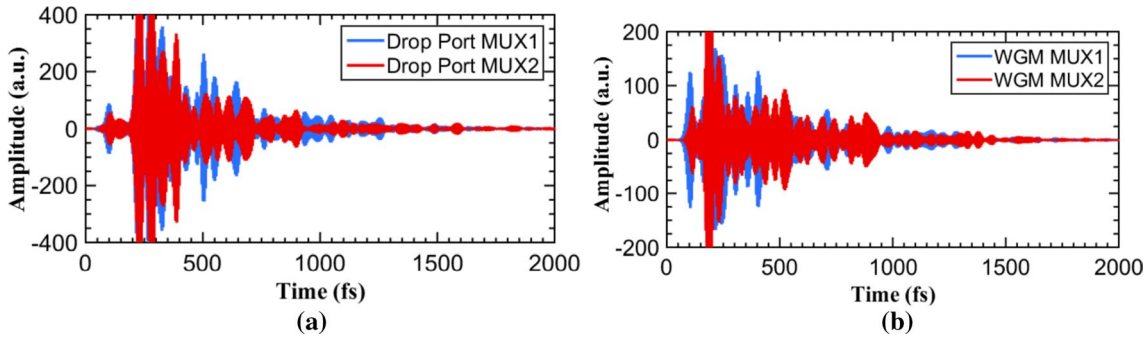

Fig. 5 Plot of the output intensity in time domain, where **a** the drop port output of MUX1 and MUX2, **b** the WGM of MUX1and MUX2

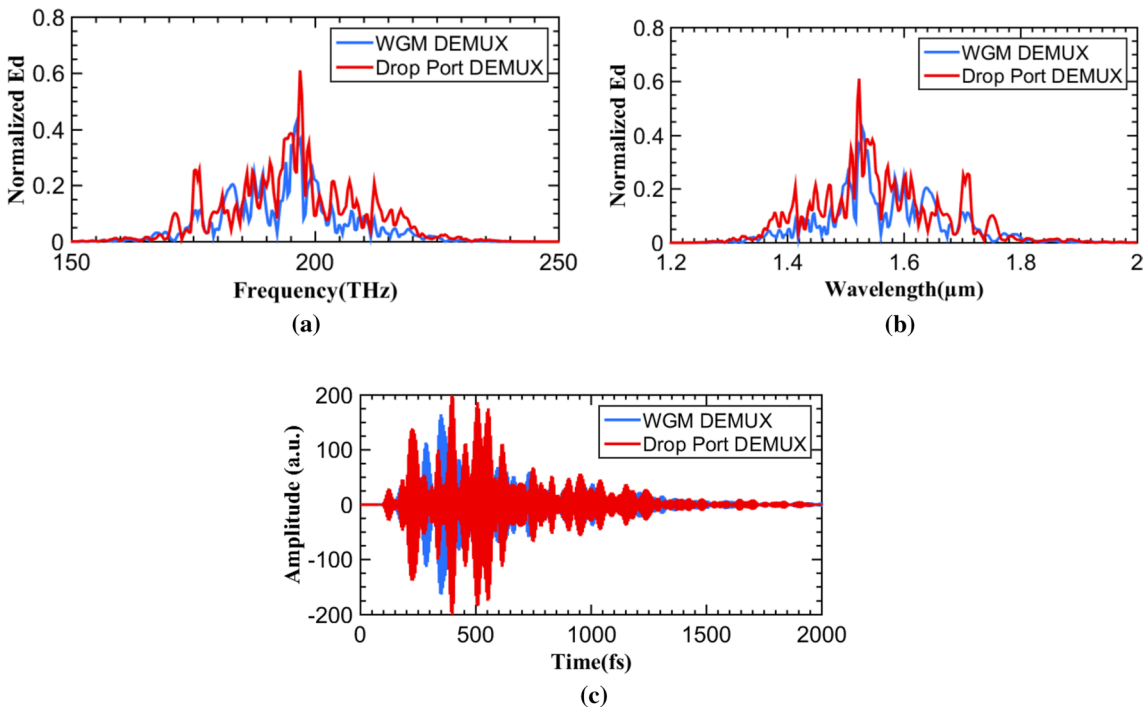

Fig. 6 Plot of the normalized electron density for DEMUX, where **a** frequency domain, **b** wavelength domain, **c** time domain. The plasma frequency is 0.72×10^{16} radsec^{-1}

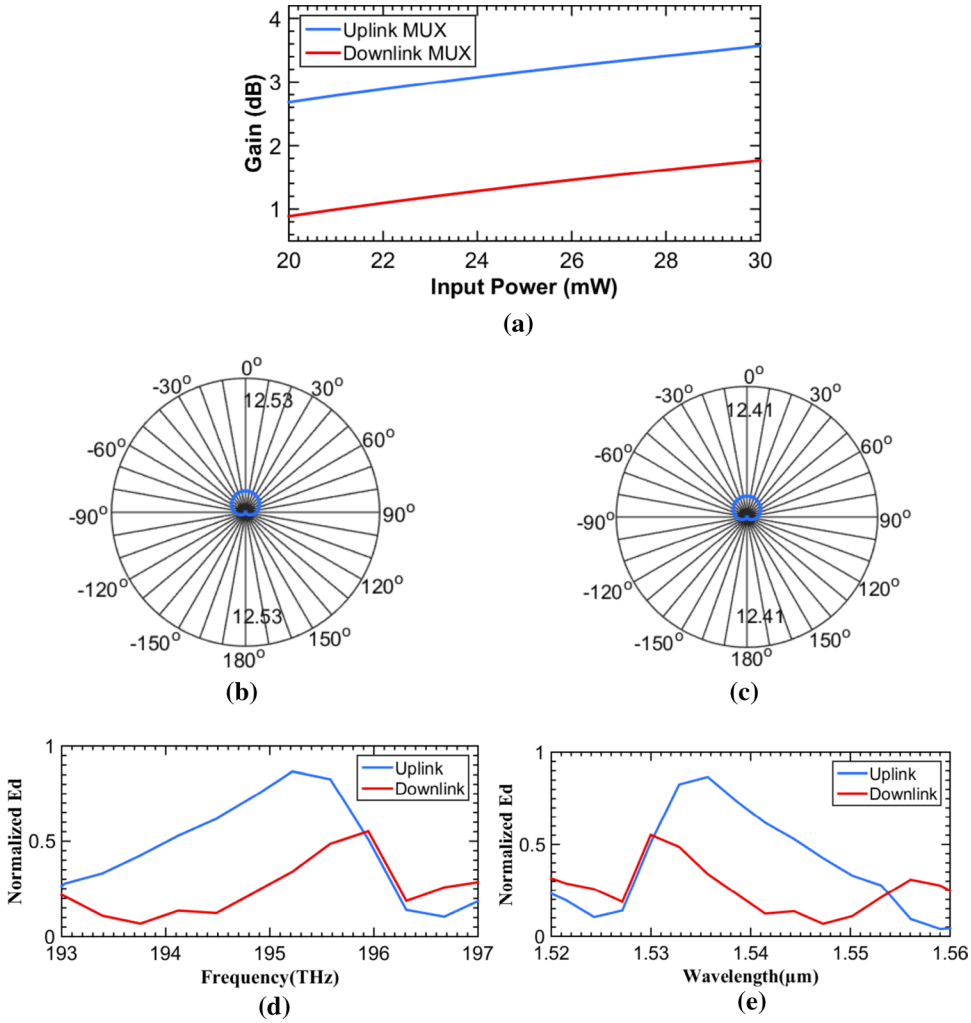

Fig. 7 Plot of the antenna profiles, where **a** gain, **b** directivity of uplink, **c** directivity of downlink, (d)WiFi uplink and downlink frequency bands, I LiFi uplink and downlink wavelength bands. The center frequency and wavelength are 195.2 THz and 195.9 THz and, 1.535 μm and 1.530 μm for uplink and downlink, respectively

transmission. The transmission validation is performed by the tested node results. Figure 8 shows the transmission capacity of DEMUX with a tested node-1 in time, wavelength, and frequency domains. The test node is simulated by six different fiber distances of 10 km, 50 km, 100 km, 200 km, 500 km, and 1000 km. The entanglement formation can be applied for security requirements, which can be performed similar to the details in reference [33]. The crosstalk calculated for two different wavelengths of 1.30 μm and 1.10 μm is shown in Fig. 9a–b. When calculating the crosstalk for 1.30 μm wavelength signal, the 1.10 μm wavelength signal acts as noise, and when calculating the crosstalk for 1.10 μm wavelength signal, 1.30 μm wavelength signal acts as noise. Figure 9c–d shows the plot of the BER (bit error rate) of the system for 1.10 and 1.30 μm wavelength signals, where the BER of 0.38 and 0.48 is achieved. It means that the BER can be neglected, in which the lower the BER, the better performance of the system is obtained. The optimum chirp rate is 2.9 GHz in the frequency domain and 2.5 nm in wavelength domain at 1000 km distance. In application, the transmission connection between lightwave and microwave can be applied by the micro-scale optical circuits.

4 Conclusion

This paper proposed a generalized MUX/ DEMUX circuit using MZI for LiFi and WiFi uplink and downlink transmission. The circuit is formed by three center microrings coupled with the two side rings. The small rings induce the nonlinearity effect into the circuit, where the WGM can be formed to excite the electrons on the grating surfaces. The gold grating embedded at the center microrings shifted the center wavelength of 1.54 μm to the Bragg wavelengths of 1.56 μm, and 1.57 μm. The working principle of the circuit is based on space–time control, where the two WGMs at MUX1 and MUX2 are used as uplink and downlink plasmonic antennas. By using the electro-optic signal conversion signals, the light beam and antenna can be applied for LiFi and WiFi uplink and downlink transmission, respectively.

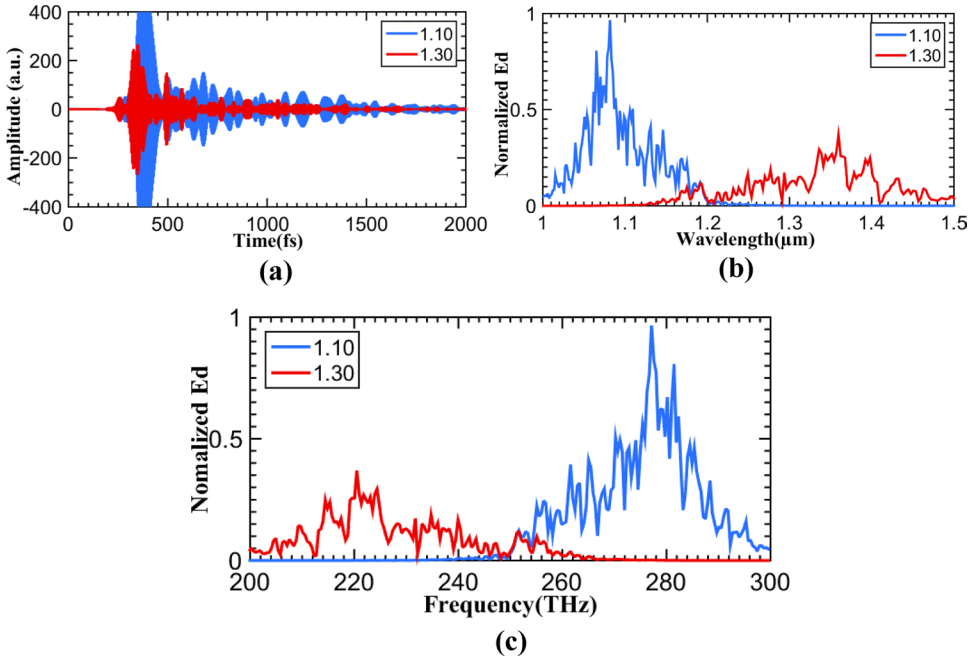

Fig. 8 Plot of the transmission capacity of DEMUX with a tested node-1, where **a** time domain, **b** wavelength domain **c** frequency domain. The shifted frequency is 3.7 GHz; the shifted wavelength is 3.7 nm

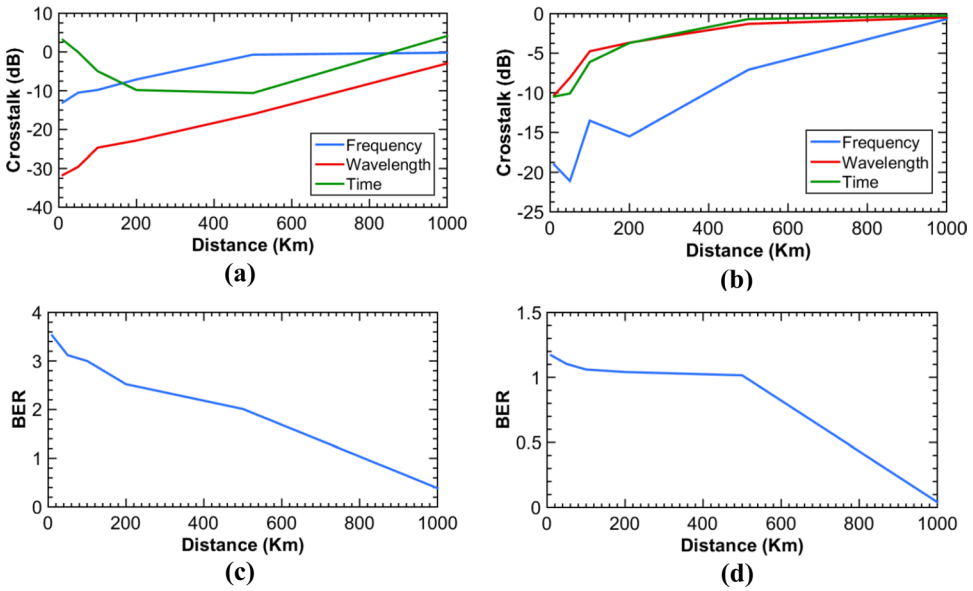

Fig. 9 Plot of the tested node outputs, where **a** crosstalk with distances for 1.10 μm, **b** crosstalk with distances for 1.30 μm, **c** BER for 1.10 μm, **d** BER for 1.30 μm. The BER results are not significant when the transmission rate is Tbit/s. The optimum shifted frequency is 2.9 GHz; the optimum shifted wavelength is 2.5 nm

Here, optical fiber is used to perform the transmission validation. The system MUX and DEMUX can be connected to the single mode-fiber cable for a transmission test. The obtained results have shown that the uplink and downlink antenna gains of 3.57 and 1.76 dB are achieved, respectively. The uplink and downlink antenna directivities of 12.53 and 12.41 are obtained. The original signal transmission is taken place by using the multiplexing in time, wavelength, and frequency domains. The optimum wavelength and frequency shifts of 2.5 nm and 2.9 GHz are obtained, and the shifts in frequency and wavelength are not significant for the digital and quantum transmission. The transmission bit rate of 2.52 Pb s^{-1} with the bit error rate (BER) of 0.38 and 0.48 has been achieved. The multiplexed bandwidths can be increased by more input space–time input sources, which can be available for future applications.

Acknowledgements The authors would like to acknowledge the research facilities from Ton Duc Thang University, Vietnam.

Author's contributions AG contributed to MATLAB results improvement, review and editing, and discussion; AEA contributed to graphic improvement and discussion; KR contributed to modeling, analysis, discussion, and final editing, PYo contributed to validation, comparing Optiwave and MATLAB results, visualization, and discussion; SP

contributed to discussion and English polishing; PYu contributed to conceptualization, supervision, review, editing and submission. All authors have read through the manuscript.

Funding Not applicable.

Declarations

Conflict of interest The authors have declared no conflict of interest.

Consent to participate All authors are pleased to participate in this article.

Consent to publish All authors give consent to publish this article.

References

1. Martinez, A., Sanchis, P., Marti, J.: Mach-Zehnder interferometers in photonic crystals. Opt. Quant. Electron. **37**, 77–93 (2005)
2. Singh, S., Singh, S.: Design of optical wavelength conversion based on cross polarization modulation effect of SOA-MZI. Opt. Quant. Electron. **52**, 122 (2020)
3. Guo, Z., Lu, L., Zhou, L., Shen, L., Chen, J.: 16 x 16 silicon optical switched based on dual-ring assisted Mach-Zehnder interferometers. J. Light wave Technol. **36**(2), 225–232 (2018)
4. Mendez-Astudillo, M., Okamoto, M., Ito, Y., Kita, T.: Compact thermo-optic MZI switch in silicon-on-insulator using direct carrier injection. Opt. Exp. **27**(2), 899–906 (2019)
5. Singh, P., Tripathi, K.D., Jaiswal, S., Dixit, H.K.: Design of all-optical buffer and OR gate using SOA-MZI. Opt. Quant. Electron. **46**, 1435–1444 (2013)
6. Soltanian, M.R.K., Amiri, I.S., Arianejad, M.M., Ahmad, H., Yupapin, P.: A simple humidity sensor utilizing air-gap as sensing part of the Mach-Zehnder interferometer. Opt. Quant. Electron. **49**, 308 (2017)
7. Wang, R., Zheng, C.-T., Liang, L., Ma, C.-H., Cui, Z.-C., Zhang, D.-M.: Multifunctional spectrum-periodic polymer MZI electro-optic switch/filter using serial-cascaded phase-generating couplers: theory, design and analysis. Opt. Quant. Electron. **44**, 337–354 (2012)
8. Lima, A.W., Jr., Sombra, A.S.B.: Graphene-based Mach-Zehnder nanophotonics interferometer working as a splitter/switch and as a multiplexer/demultiplexer. Opt. Quant. Electron. **49**, 388 (2017)
9. Kolesik, M., Matus, M., Moloney, J.V.: All-optical Mach-Zehnder-interferomter-based demultiplexier—a computer simulation study. IEEE Photon. Technol. Lett. **15**(1), 78–80 (2003)
10. Meijerink, A., Roeloffzen, C.G.H., Meijerink, R., Zhuang, L., Marpaung, D.A.I., Bentum, M.J., Burla, M., Verpoorte, J., Jorna, P., Hulzinga, A., Etten, W.V.: Novel ring resonator-based integrated photonic beamformer for broadband phased array receive antennas—part I: design and performance analysis. J. Lightw. Technol. **28**, 1 (2010)
11. Chantakit, T., Chiangga, S., Amiri, I.S., Yupapin, P.: All-optical wireless wavelength multiplexing and demultiplexing using resonant cavity. Appl. Opt. **57**(27), 7997 (2018)
12. Badraoui, N., Berceli, T.: Enhancing capacity of optical links using polarization multiplexing. Opt. Quant. Electron. **51**, 310 (2019)
13. Lan, M., Yu, S., Cai, S., Gao, L., Gu, W.: Mode multiplexer/demultiplexer based on tapered multi-core fiber. IEEE Photon. Technol. Lett. **29**(12), 979–982 (2017)
14. Mukherjee, K.: Method of implementation and application of all-optical frequency-encoded multiplexer and demultiplexer utilizing total reflectional switches (TRSs). J. Opt. **49**, 102–109 (2020)
15. Prajzler, V., Mastera, R.: Wavelength division multiplexing module with large core optical polymer planar splitter and multi-layered dielectric filters. Opt. Quant. Electron. **49**, 133 (2017)
16. Perlicki, K.: Polarization division multiplexing system quality in the presence of polarization effects. Opt. Quant. Electron. **41**, 997–1006 (2009)
17. Sung, J.Y., Hsu, C.W., Su, H.Q., Chow, C.W., Yeh, C.H.: Optical filter analyses for demultiplexing all-optical OFDM transmission systems. Opt. Quant. Electron. **47**, 2781–2792 (2015)
18. Malhotra, Y., Kaler, R.S.: Optical time division multiplexing at 160 Gbps using MZI switching. Optik **122**, 1981–1984 (2011)
19. Heish, C.-H., Lin, K.-P., Leou, K.-C.: Design of a compact high performance electro-optic plasmonic switch. IEEE Photon. Technol. Lett. **27**(23), 2473–2476 (2015)
20. Sutili, T., Rocha, P., Gallep, C.M., Conforti, E.: Energy efficient switching technique for high-speed electro-optical semiconductor optical Amplifiers. J. Lightw. Technol. **37**(24), 6015–6024 (2019)
21. Ying, Z., Dhar, S., Zhao, Z., Feng, C., Mital, R., Chung, C.-J., Pan, D.J., Soref, R., Chen, T.R.: Eelctro-optic ripple carry adder in integrated silicon photonics for optical computing. IEEE J. Sel. Top. Quant. Electron. **24**(6), 1–10 (2018)
22. Chaudhary, S., Thakur, D., Sharma, A.: 10 Gbps-60GHz RoF transmission system for 5G applications. J. Opt. Commun. **40**(3), 281–284 (2017)
23. Islam, T., Uddin, M.N.: High Speed OTDM- DWDM bit compressed network for long-haul communication. Aiub J. Sci. Eng. **18**(02), 57–65 (2019)
24. Garhwal, A., Arumona, A.E., Youplao, P., Ray, K., Amiri, I.S., Yupapin, P.: Human-like stereo sensors using plasmonic antenna embedded MZI with space–time modulation control. Chin. Opt. Lett. **19**(10), 101301–101309 (2021)
25. Li, X., Feng, X., Cui, K., Liu, F., Huang, Y.: Integrated silicon modulator based on microring array assisted MZI. Opt. Lett. **22**(9), 10550–10558 (2014)
26. Sarapat, N., Pornsuwancharoen, N., Youplao, P., Amiri, I.S., Jalil, M.A., Ali, J., Singh, G., Yupapin, P., Grattan, K.T.: LiFi up-down-link conversion node model generated by inline successive optical pumping. Microsyst. Technol. **25**, 945–950 (2019)
27. Punthawanunt, S., Aziz, M.S., Phatharacorn, P., Chiangga, S., Ali, J., Yupapin, P.: LiFi cross-connection node model using whispering gallery mode of light in a microring resonator. Microsyst. Technol. **24**, 4833–4838 (2018)
28. Pornsuwancharoen, N., Youplao, P., Aziz, M.A., Ali, J., Singh, G., Amiri, I.S., Punthawanunt, S., Yupapin, P.: Characteristics of microring circuit using plasmonic island driven electron mobility. Microsyst. Technol. **24**, 3573–3577 (2018)
29. Bahadoran, M., Amiri, I.S.: Double critical coupled ring resonator-based add-drop filters. J. Theor. Appl. Phys. **13**, 213–220 (2019)
30. Youplao, P., Sarapat, N., Pornsuwancharoen, N., Chaiwong, K., Jalil, M.A., Amiri, I.S., Ali, J., Aziz, M.S., Chiangga, S., Singh, G., Yupapin, P., Grattan, K.T.V.: Plasmonic op-amp circuit model using the inline successive microring pumping scheme. Microsyst. Technol. **24**, 3689–3695 (2018)
31. Zheng, Y., Wu, Z., Shum, P.P., Xu, Z., Keiser, G., Humbert, G., Zhang, H., Zeng, S., Dinh, X.Q.: Sensing and lasing applications of whispering gallery mode microresonators. Opt. Electr. Adv. **1**(9), 1800 (2018)
32. Mitatha, S., Pornsuwancharoen, N., Yupapin, P.P.: A simultaneous short-wave and millimeter-wave generation using a soliton pulse within a nano-waveguide. IEEE Photon. Technol. Lett. **21**, 932–934 (2009)

33. Mitatha, S., Piyatamrong, B., Tamee, K., Yupapin, P.P.: Multi-function sensors using coincidence dark-bright soliton pair in a MZI. IEEE Sens. J. **12**(5), 984–987 (2011)
34. Arumona, A.E., Amiri, I.S., Yupapin, P.: Plasmonic micro-antenna characteristics using gold grating embedded in a panda-ring circuit. Plasmonics **15**, 279–285 (2020)
35. Garhwal, A., Ray, K., Arumona, A.E., Bharti, G.K., Amiri, I.S., Yupapin, P.: Spin-wave generation using MZI embedded plasmonic antenna for quantum communications. Opt. Quant. Electron. **52**, 241 (2020)
36. Arumona, A.E., Amiri, I.S., Punthawanunt, S., Yupapin, P.: High-density quantum bits generation using microring plasmonic antenna. Opt. Quant. Electron. **52**, 208 (2020)
37. Arumona, A.E., Amiri, I.S., Punthawanunt, S., Ray, K., Yupapin, P.: Electron density transport using microring circuit for dual-mode power transmission. Opt. Quant. Electron. **52**, 213 (2020)

A. Garhwal received her PhD from Amity School of Engineering and Technology (ASET), Amity University Rajasthan, India. She was a PhD intern student at Advance Institute of Materials Science, Ton Duc Thang University, Ho Chi Minh City, Vietnam. His research interests are micro-/nano-antennas, and plasmonics.

A. E. Arumona is a PhD candidate in the Computational Optics Research Group, Advanced Institute of Materials Science, Faculty of Applied Sciences and Division of Computational Physics, Institute for Computational Science, Ton Duc Thang University, Ho Chi Minh City, Vietnam. His research interests are quantum electronics and plasmonics.

K. Ray has been a Professor of Physics and Electronics and Communication, and presently working as Head of the Department of Physics at the Amity School of Applied Sciences, Amity University Rajasthan (AUR), Jaipur, India. His current interestes are quantum deep learning, machine learninf and neural network.

P. Youplao received his D.Eng. in Electrical Engineering from King Mongkut's Institute of Technology Ladkrabang, Bangkok, Thailand, in 2013. He is an assistant professor in electrical engineering.

S. Punthawanunt received his M.Sc. in computer science from Assumption University, Bangkok, Thailand. He is currently a Dean of Faculty of Science, Kasem Bundit University, Bangkok 10250, Thailand.

P. Yupapin received the Ph.D. degree in electrical engineering from the City, University of London, UK, in 1993. He is currently the full Professor in the Department of Electrical Technology, Faculty of Industrial Technology, Institute of Vocational Education Northeastern Region 2, Sakonnakhon, Thailand. His current interestes are quantum technology, deep learning and neural network.